Hindawi
Shock and Vibration
Volume 2021, Article ID 2809467, 14 pages
https://doi.org/10.1155/2021/2809467

Research Article

Sensitivity Analysis Strategy to Assess the Salting-Out Problem during CO_2 Geological Storage Process

Jie Ren [1] **and Di Feng** [2]

[1]*College of Mechanics and Materials, Hohai University, Nanjing, China*
[2]*College of Civil and Transportation Engineering, Hohai University, Nanjing, China*

Correspondence should be addressed to Jie Ren; renjiehhu@163.com

Received 1 November 2021; Accepted 10 December 2021; Published 21 December 2021

Academic Editor: Zhanbo Cheng

The sensitivity analysis of the salting-out effect on well injectivity is a significant work in the research of geological storage of CO_2 in deep saline aquifers, which is helpful in the selection of storage sites and the design of the injection strategy. We conduct a detailed sensitivity analysis about the salting-out process using the local sensitivity method and two global sensitivity methods. Sensitivity coefficients showed that brine salinity (X_{NaCl}) has the highest sensitivity and interaction effect, the CO_2 injection rate (Q_{CO2}) has a greater influence in the early stage of the salting-out process and a smaller influence in the end stage, and the other three parameters (empirical parameters related to the pore distribution m, the liquid residual saturation in the relative permeability function S_{plr}, and the liquid residual saturation in the capillary pressure function S_{clr}) have a smaller sensitivity. This paper also analyzes the calculation amount of different sensitivity methods and suitable ways of obtaining the sensitivity coefficient and reveals the following. (1) The sensitivity coefficient changes dynamically with time, if only the sensitivity of the final state is taken into account on a long-time physical process, and some sensitive parameters during the process may be neglected. (2) The selection of the sample size should be based on the convergence of multiple calculations, and the results of the empirical calculation are uncertain. (3) The calculation of Sobol sensitivity is complicated, the results calculated by surrogate model depend on whether the sample is representative enough; on the other hand, it is feasible to use S_{ti}-S_i approximation to characterize the second-order sensitivity to reduce the computation. The research results not only reveal the sensitivity of the parameters related to the injection well salting-out problem during CO_2 storage in deep saline aquifers but also guide the calculation of global sensitivity analysis with a similar physical process.

1. Introduction

Geological storage of carbon dioxide (CO_2) is an effective way to mitigate the effect of global warming [1]. Because of its wide distribution and large storage capacity, the deep saline aquifer is considered as an effective site for large-scale CO_2 geological storage [2]. In the near and medium-term, the main interest of carbon sequestration technology is to solve the problem of low storage capacity, and in the future, deep saline aquifers are the main technology of carbon sequestration [3]. Currently, CO_2 geological storage has not been commercialized due to the high construction cost. There are broad prospects for CO_2 geological sequestration in deep saline aquifers because lots of countries have formulated strict carbon emission reduction plans [4] and the implementation of carbon pricing makes CO_2 sequestration profitable.

The dissolution of CO_2 in water and the dissolution of water in CO_2 occur at the same time in the CO_2-brine system [5]. Although the solubility of water in CO_2 is low under site conditions, this dehydration process cannot be ignored when a large amount of dry CO_2 fluid is continuously injected into the rock formation [6]. When CO_2 is injected into the deep saline aquifer with higher salinity, it removes the

water from the brine and increases the concentration of the brine; in turn, salt crystallization occurs when the concentration of the brine reaches the saturation limit [6–9].

At present, there are few site projects sealed in deep saline aquifers. According to statistics, large-scale site projects will enter the explosive period after 2020 [3]. Most of the current research on the geological storage of CO_2 in deep saline aquifers focuses on the exploration of CO_2 migration law, storage mechanisms, and risk assessment of leakage [10–14]. The monitoring data from the site project show that the salt precipitation near the well is part of the low permeability zone, which causes the accumulation of injection pressure and reduces the CO_2 injectivity [15]. Therefore, with the development of a large number of CO_2 storage projects in the deep saline aquifers, it is necessary to screen and evaluate the potential sites from the point of view of the impact of salting out, to provide a basis for site storage potential evaluation and site selection.

The main purpose of studying the phenomenon of salting out is to study the effect of salt precipitation on the permeability of rock formation. Verma and Pruess [16] proposed to transform the relationship between porosity and permeability into the relationship between solid saturation (S_s) and permeability, and the value of S_s indicates the percentage of volume of NaCl crystals in the pores of the rock. According to the conservation of mass, Pruess [17] gives a method for calculating the S_s value, so that the study of salting out can be transformed into quantitative research of S_s.

Sensitivity analysis of the parameters affecting S_s of the injection well is the focus of the research on the salting-out effect at present. Miri and Hellevang [18] summarize the research results using simulation studies for the salt precipitation induced by CO_2 injection. These numerical simulation studies consider sensitivity parameters including injection rate, initial brine saturation, salinity, water content, capillary pressure, relative permeability, temperature, and permeability. [19–25]. The above studies are all local sensitivity analysis considering a single factor and cannot give the sensitivity comparison among the parameters and cannot get the effect of the interaction between the parameters on the S_s.

The global sensitivity analysis method can not only examine the influence of input variables on response variables but also examine the interaction of input parameters and the influence of multiparameters on response variables. The commonly used global sensitivity analysis methods include the Morris method [26] and the Sobol method [27] based on variance analysis. Jung et al. [28] and Wainwright et al. [29] conducted a global sensitivity analysis using the Morris method to evaluate the sensitivity of the leakage signal (pressure disturbance) to the parameters of the geological storage model of CO_2. Zheng et al. [30, 31] carried out a global parameter sensitivity analysis of the CO_2 migration process in deep saline aquifers and compared the Morris method, the Sobol method, and other sensitivity analysis methods. It is found that the sensitivity arrangement of the input variables is different when different response variables are selected. Sobol's method has high accuracy, but the amount of calculation is too large. Wang et al. [32] conducted a global sensitivity analysis to evaluate the sensitivity of clogging signals (S_s) to model parameters, but they use the kriging surrogate model to simplify the migration dissolution process of CO_2 injection into the deep saline aquifers to simplify the calculation of Sobol's method.

In this study, we conduct a more detailed analysis, using the same salting-out forward model developed by Wang et al. [32]. Firstly, we conduct a sensitivity analysis based on the local sensitivity method and two global sensitivity methods. Then, the influence of the selection of calculation parameters on the results of sensitivity analysis is discussed. An additional interpretation is provided for the local and global sensitivity methods. Finally, differences between the Sobol methods calculated from hydrogeological forward simulation and surrogate model are compared. The research results not only reveal the sensitivity of the parameters related to the injection wells salting-out problem during CO_2 storage in deep saline aquifers but also guide the selection of calculation parameters for similar sensitivity analysis, such as the process of heat extraction, energy storage, and evolution analysis of geological parameters [33–36].

2. Methodology

2.1. Modeling Approach of the Salting-Out Process. A radial geological model was built to simulate the salting-out process. The model used for sensitivity analysis is the same as Wang et al.'s model [32]. Assume that supercritical carbon dioxide ($scCO_2$) is injected into a homogeneous, anisotropic deep saline aquifer at a constant injection rate (Q_{CO2}). The thickness of the storage layer is 100 m, and the horizontal distance is 2,500 m. The radius of the injection well is 0.3 m, and it is 11.5 m from the bottom of the model. The one-quarter concept model is shown in Figure 1. In the horizontal direction, the injection well is the first unit with a unit size of 0.3 m, followed by 50 logarithmic size increasing units; in the vertical direction, the injection well is 11.5 m above the center of the bottom boundary element with a thickness of 1 m, and the thickness of the bottom and top units is 2 m. Other parts are evenly divided into units with a thickness of 5 m. The specific divided grid is shown in Figure 2; the upper and lower borders and right borders are sealed as no-flow boundary conditions. The parameters of the model used for simulation are given in Table 1.

The TOUGH2/ECO2N module is used to simulate CO_2 migration in deep saline aquifers and the salting-out process due to the miscibility of water and CO_2 [17], and the injection time is set at 100 days. In the sensitivity analysis, we choose five parameters as input parameters: CO_2 injection rate (Q_{CO2}), salinity (X_{NaCl}), empirical parameters related to pore distribution (m), liquid residual saturation in the relative permeability function (S_{plr}), and liquid residual saturation in the capillary pressure function (S_{clr}). Table 2 shows the ranges of reference parameter for sampling during sensitivity analysis. We assume a uniform distribution within the range of each parameter. From current researches, the salting-out problem can clog the gas flow path and reduce the CO_2 injectivity [24, 39, 40]. According to the VP model, the gas injectivity in the salting zone varies with

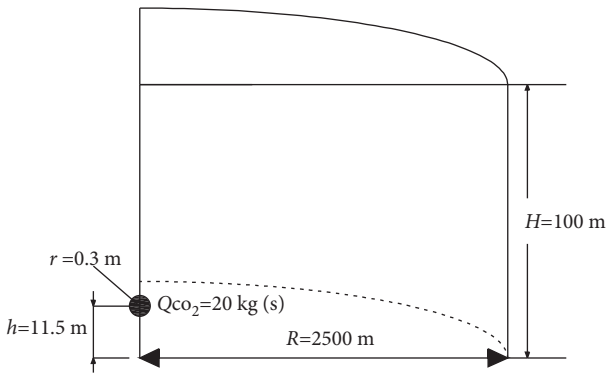

Figure 1: Concept radial geological model.

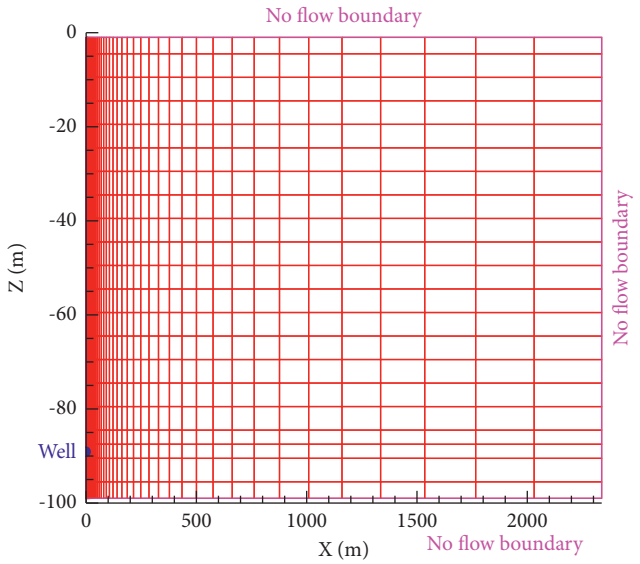

Figure 2: Reservoir mesh diagram and boundary conditions.

the solid saturation value S_s [16], so S_s is used to map the CO_2 injectivity and as the response variable for the sensitivity analysis. We set the injection unit as an observation point and S_s as a function of time in the reference case shown in Figure 3.

Figure 3 presents the time evolution of S_s at the observation point, from 10 seconds to 100 days after injection of $scCO_2$, the value of S_s keeps constant, which means a complete salting-out situation. It takes saline in the well unit 1.6×10^5 s to reach the saturation limit, and the salt precipitation accumulation process keeps about 1.2×10^5 s.

2.2. Sensitivity Analysis of the Salting-Out Problem. The sensitivity coefficients show the impact of parameter change on the calculated system behavior at the observation point. We perturb five parameters: Q_{CO2}, X_{NaCl}, m, S_{plr}, and S_{clr}; the number of parameters (n_k) equals 5. S_s is used as the response variable for sensitivity analysis, we consider a set of n_k parameters denoted by $\{x_i | i = 1, \ldots, n_k\}$, and the forward simulation output $y = f(\{x_i\})$, where f represents a forward model calculated by the TOUGH2 simulator [41], as shown in Section 2.1.

We discuss three sensitivity analysis methods, including the local sensitivity method, the Morris global sensitivity method, and the Sobol global sensitivity method. Forward simulation is taken by the TOUGH2 code; the inverse modeling capabilities for the TOUGH2 detailed calculation of the three models are developed by Wainwright et al. [29].

Local sensitivity analysis only tests the effect of a single parameter on the model; it can be calculated by the following equation:

$$S_i^{\text{local}} = \frac{\tau_{x,i}}{\tau_y} \frac{\partial y}{\partial x}\Big|_{x_i^*} = \frac{\tau_{x,i}}{\tau_y} \frac{f\left(x_1^*, L, x_i^* + nx_i, L, x_{n_k}^*\right) - f\left(x_1^*, L, x_{n_k}^*\right)}{nx_i}, \tag{1}$$

where S_i^{local} is the local sensitivity coefficient for parameter i, x_i^* is the reference parameter value, Δx_i is a parameter increment, $\tau_{x,i}$ is the parameter-scaling factor, and τ_y is the output-scaling factor [42]. This coefficient can be used to identify the parameters that most strongly affect the behavior of the system at the actual or potential observation points.

A global sensitivity analysis method can test the interaction between parameters, and it can test the effect of multiple parameters, which change concurrently with the response variable. The conventional approach to performing global sensitivity analysis is the Morris sensitivity test method and Sobol's sensitivity test method. Morris [26] proposed a data screening method that can select parameters that have a low impact on the results and reduce the number of analysis variables.

The Morris method is one of the global sensitivity analysis methods. The elementary effect of parameter x_i is calculated by the following equation [29]:

$$\text{EE}_i = \frac{1}{\tau_y} \frac{f\left(x_1^*, L, x_i^* + n, L, x_{n_k}^*\right) - f\left(x_1^*, L, x_{n_k}^*\right)}{n}, \tag{2}$$

where EE_i is the elementary effect of parameter x_i, $\Delta = n_p/\{2(n_p - 1)\}$ is the fixed increment from the unit interval [0, 1], each parameter range is scaled to the interval [0, 1], partitioned into $(n_p - 1)$ equally-sized intervals, and each parameter take on values from $\{0, 1/(n_p - 1), 2/(n_p - 1), \ldots, 1\}$, where n_p is the number of sampling points in the interval [0, 1] [26], based on which the elementary effects (EE) and variance (STD of EE) are calculated; reflecting the relative parameter importance, as well as linearity and correlation, EE and STD of EE are two sensitivity coefficients in the Morris method. Nonlinear effects and interaction effects cannot be separated using this method [26].

The Sobol method is a quantitative global sensitivity analysis method based on a variance analysis first proposed by Sobol [27]. The sensitivity of a single input parameter can be evaluated by calculating the contribution of that parameter to the output variance, and the cross-sensitivity of multiple input parameters can also be evaluated by calculating the contribution of multiple input parameters to the output variance. The basic equations are given as follows:

Table 1: The parameters of the model in the simulation.

Parameter type	Parameter value
Hydrogeological parameters	$k_x = 100$ mD, $k_y = 100$ mD, $k_z = 100$ mD, porosity (ϕ) = 12%
Initial condition	Pressure (P) = 10 MPa, temperature (T) = 45°C, gas saturation (S_{gas}) = 0%, salinity (X_{NaCl}) = 10%Q_{CO2} = 20 kg/s
Parameters in the relative permeability equation (van Genuchten–Mualem model [37, 38])	$m = 0.472$, $S_{lr} = 0.20$, $S_{gr} = 0.05$, $S_{ls} = 1$
Parameters in the capillary pressure equation (van Genuchten function [38])	$m = 0.472$, $S_{lr} = 0.05$, $P_0 = 19.61$ kPa, $P_{max} = 10$ MPa, $S_{ls} = 0.999$

Table 2: The range of reference parameters.

Parameter	Range
Q_{CO2}	5~25 (kg/s)
X_{NaCl}	5~25 (%)
M	0.217~0.557
S_{plr}	0.10~0.30
S_{clr}	0.0~0.20

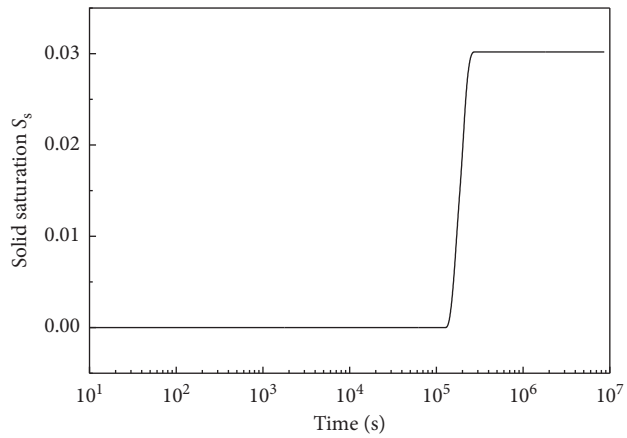

Figure 3: Time evolution of solid saturation at the observation point (injection well).

$$S_i = \frac{\mathbf{V}[\mathbf{E}[Y|X_i]]}{\mathbf{V}[Y]},$$
$$S_{ti} = 1 - \frac{\mathbf{V}[\mathbf{E}[Y|X_{-i}]]}{\mathbf{V}[Y]}, \quad (3)$$

where S_i is the first-order sensitivity value, S_{ti} is the total sensitivity value, $\mathbf{E}[\cdot]$ is the mean, $\mathbf{V}[\cdot]$ is the variance, X_i is the random system parameter, Y is the random system response, and X_{-i} is all random system parameters except X_i. The calculation method was proposed by Sobol [27] and modified by Saltelli et al. [43].

3. Results and Discussions

3.1. Reasonable Calculation of Sample Size Using Different Sensitivity Methods. Forward analysis was implemented 6 times (the formula is $n_k + 1$) for the local sensitivity method. The Morris method can be considered as an extension of the local sensitivity method by comparing (1) and (2); one local sensitivity simulation is 1 path (n_B) in the Morris simulation. The Morris method requires multiple sampling frequencies to calculate the average value. Figure 4 shows the mean EE and STD of EE at 100 days for each parameter as a function of n_B with $n_p = 4$; the mean EE and the STD of EE appear to stabilize after 200 n_B. In the case of a lower path's situation, although the value of the mean EE and the STD of EE is not stable, we can also distinguish the magnitude of the parameter's sensitivity and assess the importance of parameters.

In the Sobol method, we only need to determine n_s, where n_s is the number of sets of n_k dimensional parameter vectors from Monte Carlo sampling. Figure 5 shows S_i and S_{ti} for each parameter at 100 days as a function of n_s. From the figure, we can see that S_i and S_{ti} require several thousand n_s to stabilize (larger than 2,000 sets).

Due to the randomness of the Morris method, it is easy to meet the error during the 1 path calculated, and it is necessary to do multiple paths calculations to reduce the error. Saltelli et al. [44] present an experienced range of paths 4~10 to easily obtain Morris calculations. Most scholars did not consider the effects of the paths on the Morris sensitivity analysis, and they always use the experience paths, such as $n_B = 4$ (Wang et al. [32]), $n_B = 10$ (Zheng et al. [31]), $n_B = 10$ (Wainwright et al. [45]), and $n_B = 25$ (Finsterle [46]). This way would bring some errors in the Morris sensitivity analysis, and the error was discussed in Section 3.4. As to n_s in Sobol sensitivity analysis, most researchers also chose the experienced value of n_s to do the calculation, such as $n_s = 300$ in Wainwright et al. [45]; it is also important to study the effect of n_s on sensitivity coefficients and get the big enough n_s to keep the sensitivity coefficient converged.

For the global sensitivity analysis coefficient, the confidence intervals are shown so that we can evaluate the parameter coefficient uncertainty with the given number of simulations (draw error band). In the Morris method, the standard error of the mean (SEM) of EE, defined as $\mathrm{SEM} = \mathrm{STD}/n_B^{0.5}$ [26], is used to calculate the confidence interval of the mean EE. In the Sobol method, the confidence interval of S_i is given as $\tanh\{\mathrm{arctanh}(S_i) \pm 1.96\mathrm{SE}\}$ [29], where SE is the standard error given by $\mathrm{SE} = (n_s - 3)^{-0.5}$. We chose $n_B = 200$ and $n_s = 1{,}000$ according to Figures 4 and 5 to ensure that the sensitivity of the calculated values is stable; the 95% confidence intervals of mean EE and S_i are given below.

Figure 6(a) shows a minor error band of the parameter sensitivity coefficient. This is because of the large number of n_B in the equation $\mathrm{SEM} = \mathrm{STD}/n_B^{0.5}$. The width of the confidence interval increases for small S_i (Figure 6(b)),

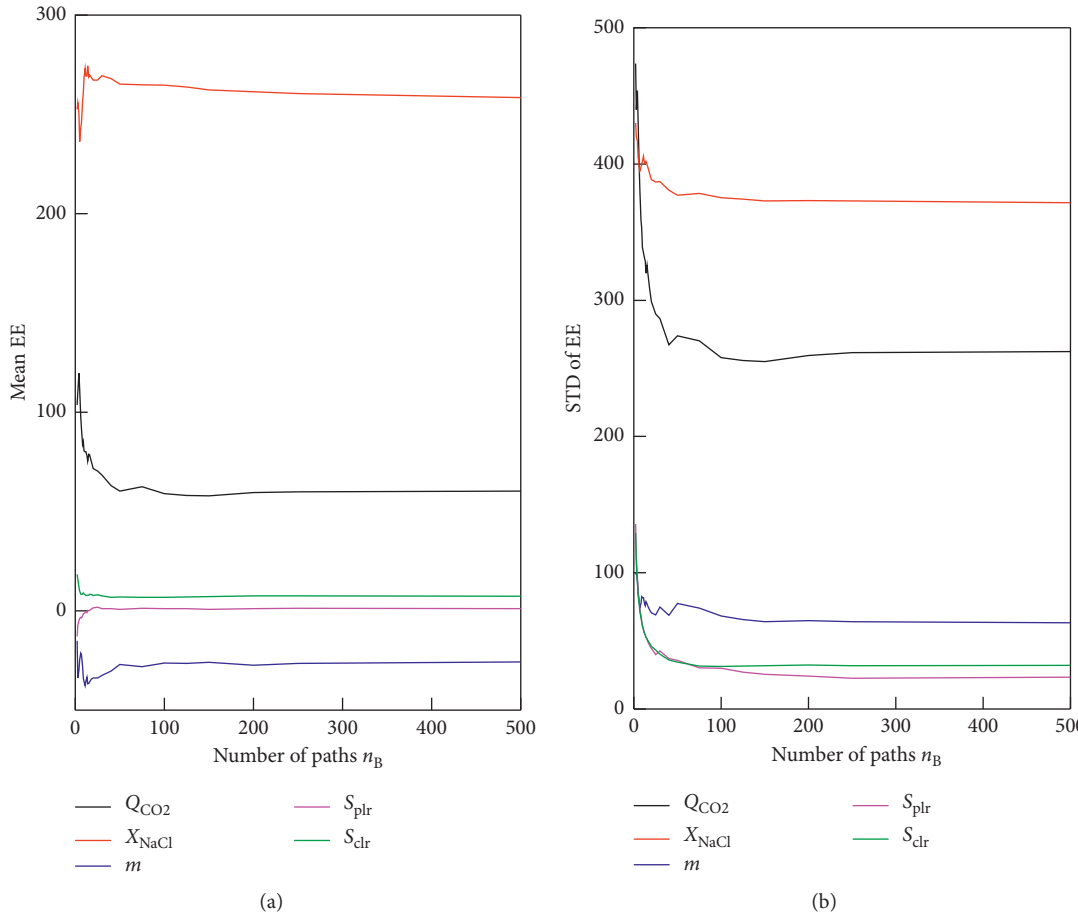

Figure 4: (a) Mean EE and (b) STD of EE as a function of the path (n_B).

implying that more simulations are required to rank the low-sensitivity parameters. The relationship between the sensitivity coefficient and n_B, the relationship between sensitivity coefficient and n_s, and the plot of sensitivity coefficient with the confidence intervals help to get the credible sensitivity coefficient.

3.2. Times Evolution of Sensitivity Coefficient with Different Sensitivity Methods

3.2.1. Local Sensitivity Method. The relationship between the local sensitivity coefficient of each parameter and time is given in Figure 7.

Figure 7(a) shows the time evolution of the sensitivity coefficient of the local sensitivity analysis method. For easier comparison, Figure 7(b) shows the absolute values of the local sensitivity coefficient: $|S_i^{\text{local}}|$, which could represent the magnitude of parameter effects. As shown in Figure 7, X_{NaCl} is the most influential parameter at the early time, and Q_{CO2} has a dominant effect afterward, m has the smallest effect, and S_{plr} and S_{clr} have an intermediate effect. The sensitivity to Q_{CO2}, S_{plr}, and S_{clr} decreases later, the sensitivity to m increases later, but the sensitivity to X_{NaCl} stays constant. At the end of the injection process, X_{NaCl} is still the most influential, but S_{clr} occupies the second position. The sensitivity of Q_{CO2}, S_{plr}, and m remain at a lower sensitivity coefficient after 2.79×10^5 s; the corresponding precipitation does not increase in Figure 3.

3.2.2. Morris Sensitivity Method. In the Morris method, the number of partitions (n_p) and the number of paths (n_B) are the two parameters that determine the result of the sensitivity analysis. The premise of getting an accurate global sensitivity analysis is to investigate the influence of these two parameters. The influence of n_B has been researched in Section 3.1. Figure 8 shows the influence of n_p, the mean EE, and the STD of EE stabilized from 4 to 40 partitions, which means that n_p has a small impact on the stability of both mean EE and STD of EE in this study. From the above studies, the mean EE and STD of EE would converge when $n_B = 200$ and $n_p = 4$. The Morris sensitivity analysis results are shown in Figure 9.

Figure 9 shows the time evolution of the mean elementary effect from the Morris sensitivity analysis method. The number of simulations is 1,200 (the formula is $n_B \times (k+1)$). The mean EE represents the average effect of each parameter on the parameter space (Figure 9(a)), the mean |EE| is used to identify the noninfluential factors (Figure 9(b)), and the STD of EE is used to identify interaction effects (Figure 9(c)).

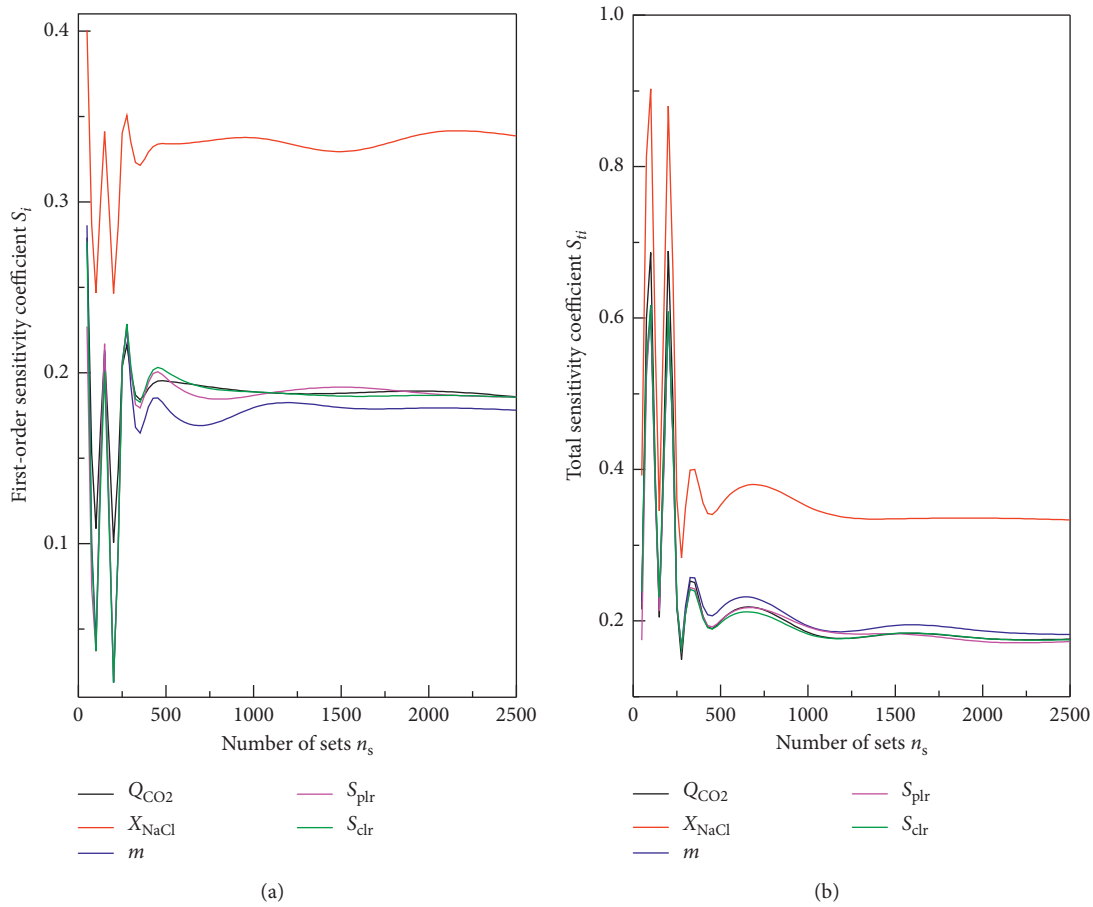

FIGURE 5: (a) S_i and (b) S_{ti} as functions of sets (n_s) using the Sobol method.

In Figure 9(b), Q_{CO2} is the most influential at the early time, and X_{NaCl} has a dominant effect afterward. The sensitivity to X_{NaCl}, m, S_{plr}, and S_{clr} increases later, but the sensitivity to Q_{CO2} decreases later. At the end of the injection process, X_{NaCl} still has a dominant effect. The effect of Q_{CO2} is reduced to a similar extent as that of m, and the sensitivity of S_{plr} and S_{clr} keeps a lower sensitivity coefficient.

The sensitivity coefficient of Q_{CO2} has different trends with other parameters. As seen in Figure 9(a), the sensitivity coefficient of Q_{CO2} is positive at the early stage and then decreases to a negative value, which means that Q_{CO2} has a positive correlation with S_s at the early time, and Q_{CO2} has a negative correlation with S_s at the later stage. In the early time, dry CO_2 injection into deep saline aquifers would bring H_2O into the CO_2 flow, and the change of Q_{CO2} leads to the same change trend of H_2O loss of brine water, which means the positive correlation. In the process of continuous injection of CO_2, the water saturation gradually decreases and the capillary pressure would increase; as seen in Figure 10, the capillary pressure in the pore would prevent further H_2O loss; this is the reason for the reduced sensitivity coefficient. The gas saturation of the rock formation gradually increases, generating a capillary pressure in the direction of the injection well, which causes the saline water to flow back to the injection well when the capillary pressure gradually increases and exceeds the displacement pressure (as shown in Figure 11). During the brine backflow process, the change in Q_{CO2} leads to different changes in S_s, causing a negative correlation [25]. The research in this paper shows that the sensitivity coefficient can be changed with time before the salting-out process is stable and the influence of the parameter on the response variable is positive or negative. Researchers should consider the dynamic change of the sensitivity index when performing a similar sensitivity analysis, in particular, considering a long-time physical process.

3.2.3. Sobol Sensitivity Method. We take $n_s = 2{,}000$ to keep S_i and S_{ti} index stable and then conduct the Sobol global sensitivity analysis; the results are shown in Figure 12.

Figure 12 shows the time evolution of the sensitivity index of the Sobol method with 14,000 simulations (the formula is $n_s \times (k+2)$). Figure 12(a) shows the first-order effect excluding the interaction effect (S_i). Figure 12(b) shows the total sensitivity index of the X_i parameter, including the interaction effect, and is used to identify parameters with negligible effects (S_{ti}). Figure 12(c) shows the difference between S_{ti} and S_i as a function of time, identifying the interaction effects. Due to the variance based on (2) and (3), the sensitivity coefficient of S_i and S_{ti} will remain positive for all time (Figure 12(a) and Figure 12(b)). In

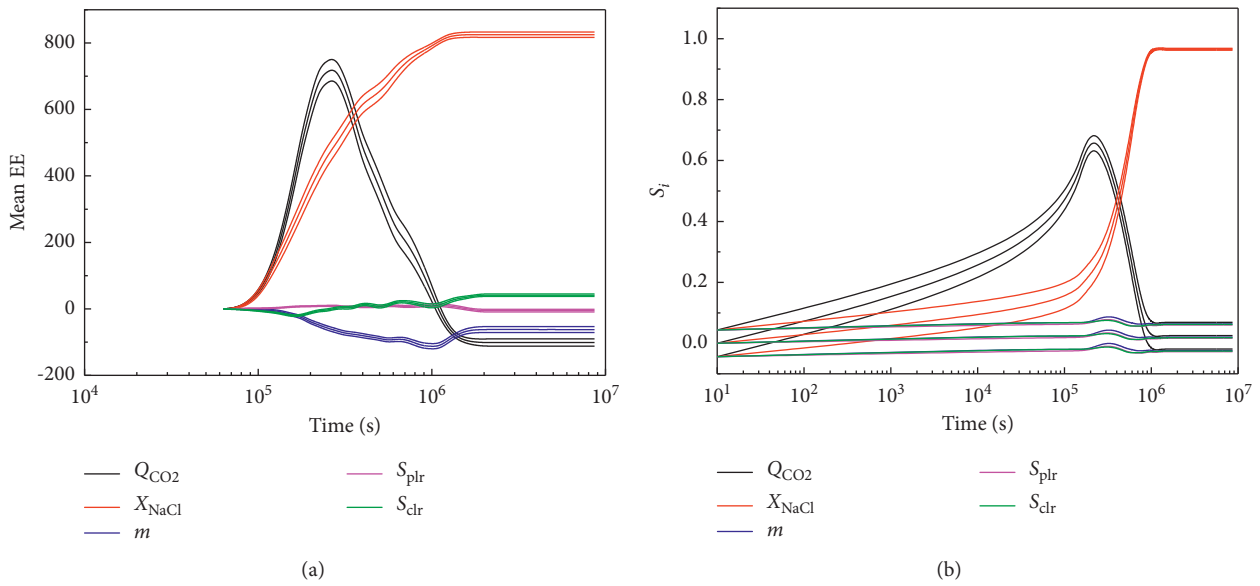

Figure 6: Time evolution of sensitivity index: (a) mean EE; (b) S_i, the thin lines represent the 95% confidence intervals.

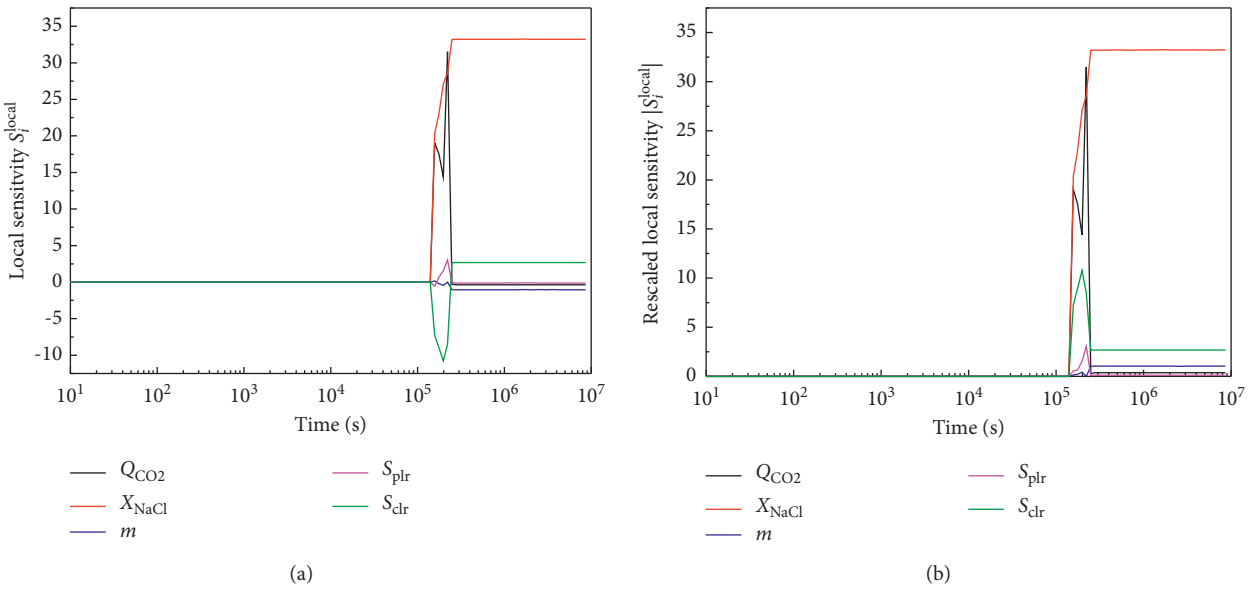

Figure 7: Time evolution of local sensitivity coefficient: (a) local sensitivity coefficient; (b) absolute values of the local sensitivity coefficient.

Figure 12(a), the largest effect of Q_{CO2} at early times can be seen, and X_{NaCl} has a dominant effect afterward. The sensitivity to Q_{CO2} and X_{NaCl} increases later, and the sensitivity to Q_{CO2} decreases to the stable value, but the sensitivity to X_{NaCl} increases to the stable value at the end of time. The patterns of the three low-influential parameters (m, S_{plr}, and S_{clr}) are similar to each other throughout the time. At the end of time, the patterns of Q_{CO2} and X_{NaCl} are similar in Figure 12a and Figure 12(b), suggesting that a change in any of these two parameters would have a significant impact on S_s even without taking into account the effects of the interaction. The ranking of low sensitivity parameters (m, S_{plr}, and S_{clr}) importance is not easily recognized than S_i^{local} in the local sensitivity analysis and mean EE in the Morris sensitivity analysis. According to the results of the confidence interval in Section 3.1, more simulations are required to rank the low-sensitivity parameters.

All parameters show interaction effects at the early time since S_{ti}-S_i is larger than 0 (Figure 12(c)). The S_{ti}-S_i decreases later and stabilizes at a low value, indicating a low interaction effect at the end times. The patterns of the S_{ti}-S_i in the Sobol method are different from the patterns of the STD of EE in the Morris method; this is because STD of EE includes both the nonlinear effects and interaction effects, but S_{ti}-S_i represents only the interaction effects [29]. Comparing Figure 9(c) with Figure 12(c), Q_{CO2} and X_{NaCl} have an abnormal trend in Figure 9(c), and the sensitivity coefficient is much higher than the other three parameters, which

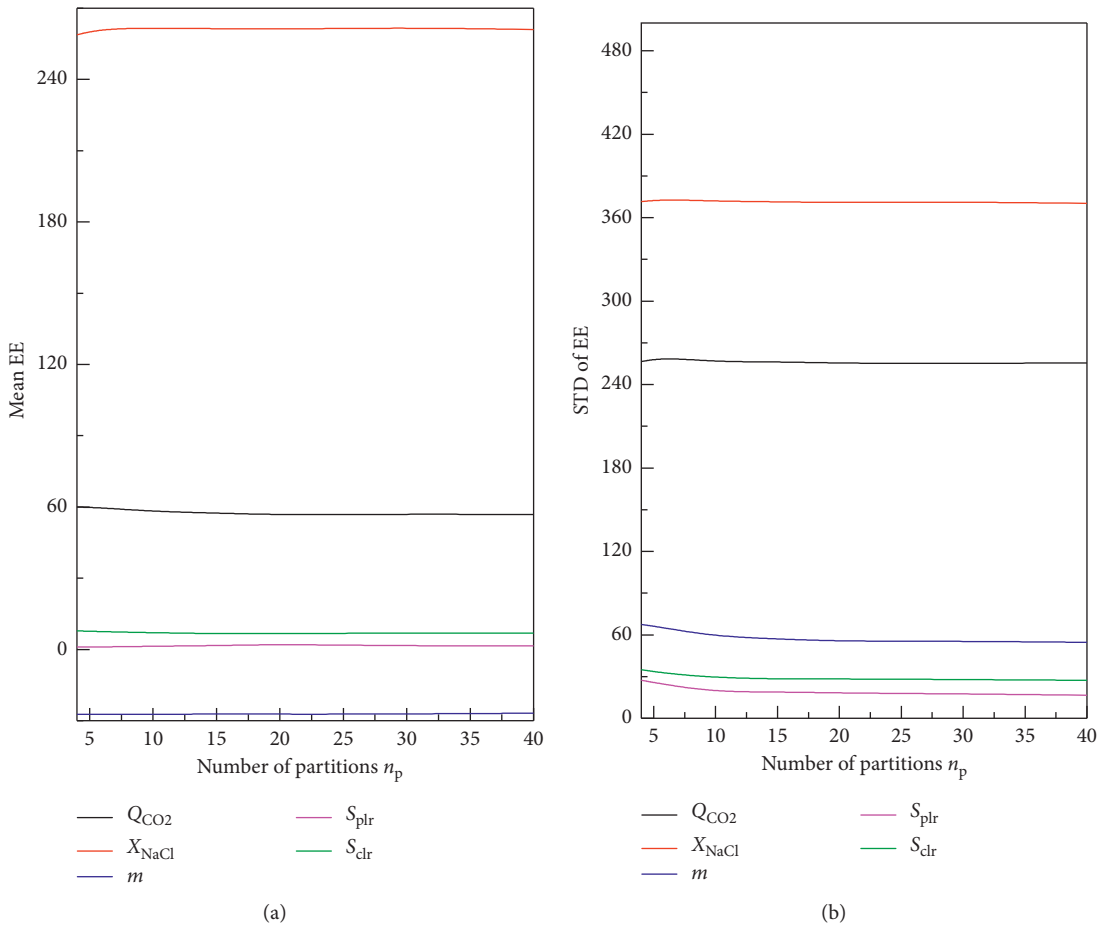

Figure 8: (a) Mean EE and (b) STD of EE as a function of partition (n_p).

indicate significant nonlinear effects of Q_{CO2} and X_{NaCl}. Comparison of STD of EE and S_{ti}-S_i helps to get a deep understanding of the sensitivity coefficient of the parameter. The nonlinear effect of Q_{CO2} can be seen in Wang et al. [32], it is mainly due to the critical value of Q_{CO2}, which controls the backflow phenomenon in the salting-out problem.

3.3. Uncertainly of Morris Results about Different Path Choice. Figure 13 shows the Morris global sensitivity analysis of S_s near the injection well, the traditional sensitivity coefficient is calculated by the equation $d_i = \Delta f(\Delta x_i)/\Delta x_i$ (Figure 13(a)). The difference in coordinate values is due to the introduction of the scaling factor $\tau_{x,i}/\tau_y$ during the sensitivity calculation of Figure 13(b), which helped to avoid a wide range of axes and plot closer and useful graphs [47].

The number of paths in Figure 13(a) is equal to 4, the descending order of the mean EE is X_{NaCl}, Q_{CO2}, m, S_{clr}, and S_{plr}, and the descending order of the STD of EE is Q_{CO2}, S_{clr}, S_{plr}, m, and X_{NaCl} [32]. Under the same path (equal to 4) and time (100 days) conditions, the results in Figure 13(b) are quite different from those in Figure 13(a), especially the STD of EE of the parameter X_{NaCl}. X_{NaCl} has a dominant interaction or nonlinear effect in Figure 13(b), but it has the lowest interaction or nonlinear effect in Figure 13(a). This is because the larger uncertainty of the initial parameters is selected because of the smaller number of paths. The sensitivity analysis result becomes more stable as the number of paths increases (Figure 13(b)). When the number of paths is 500, the descending order of the mean EE is X_{NaCl}, Q_{CO2}, S_{clr}, S_{plr}, and m and the descending order of the STD of EE is X_{NaCl}, Q_{CO2}, m, S_{clr}, and S_{plr}. This result is more accurate than Figure 13(a) carried out by Wang et al. [32].

3.4. Comparison of Sobol Results between the Physical Model and Surrogate Model. If the model has a simple and explicit mathematical expression $f(x)$, the sensitivity of Sobol can be calculated by the analytic method. If the model does not have a simple mathematical expression, to be able to extract a large number of samples while reducing the amount of computation, in one manifold method, the surrogate model [48, 49] is used instead of the physical model to calculate the response variable S_s, and then the Sobol sensitivity is calculated by Monte Carlo method [44]. In this paper, the sensitivity coefficient is calculated by real forward simulations instead of the calculation of the sensitivity coefficient coming from the Kriging surrogate model in Wang et al. [32]. The results of the comparison are shown in Figure 14.

Figure 14(a) and Figure 14(b) show the first-order and total sensitivity coefficients of the salting-out model parameters, respectively. First of all, these two figures have a similar pattern

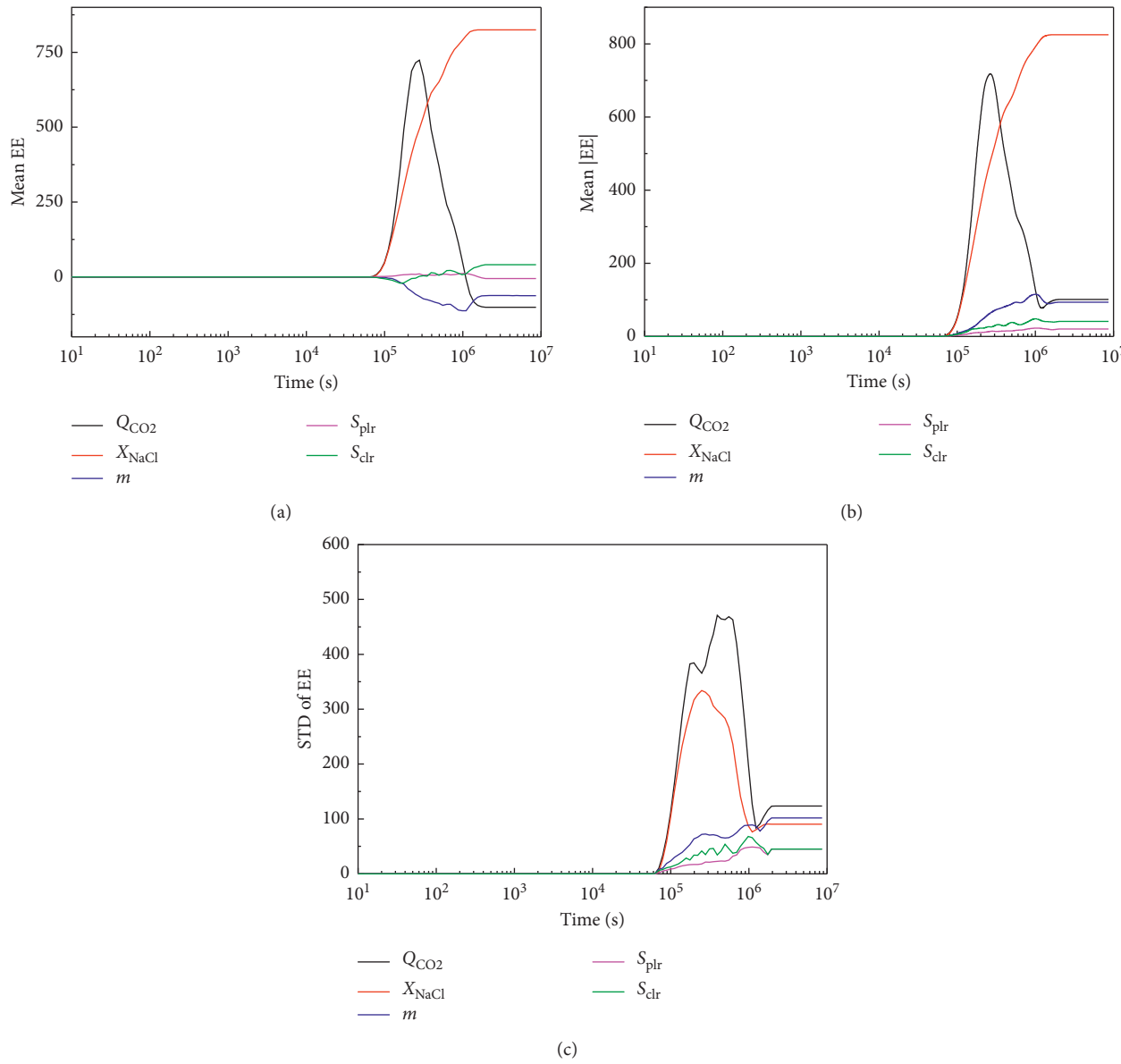

Figure 9: Time evolution of the Morris sensitivity index: (a) mean EE; (b) mean |EE|; (c) STD of EE.

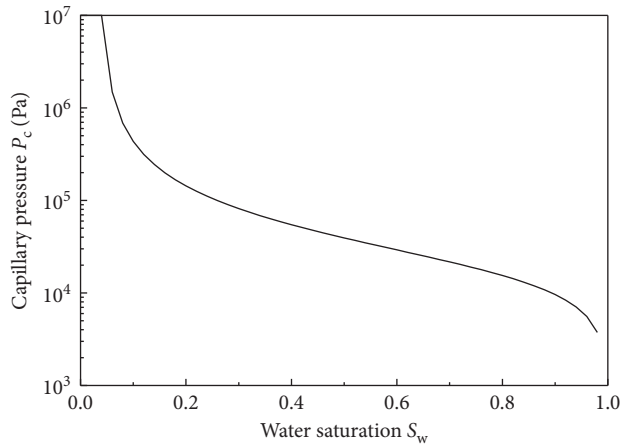

Figure 10: Capillary pressure curve.

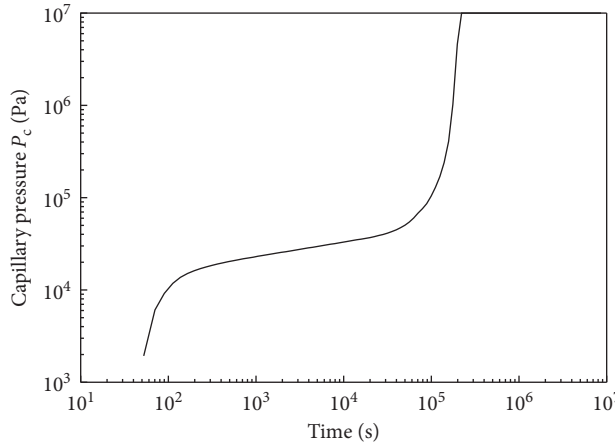

Figure 11: Time evolution of capillary pressure at the observation point.

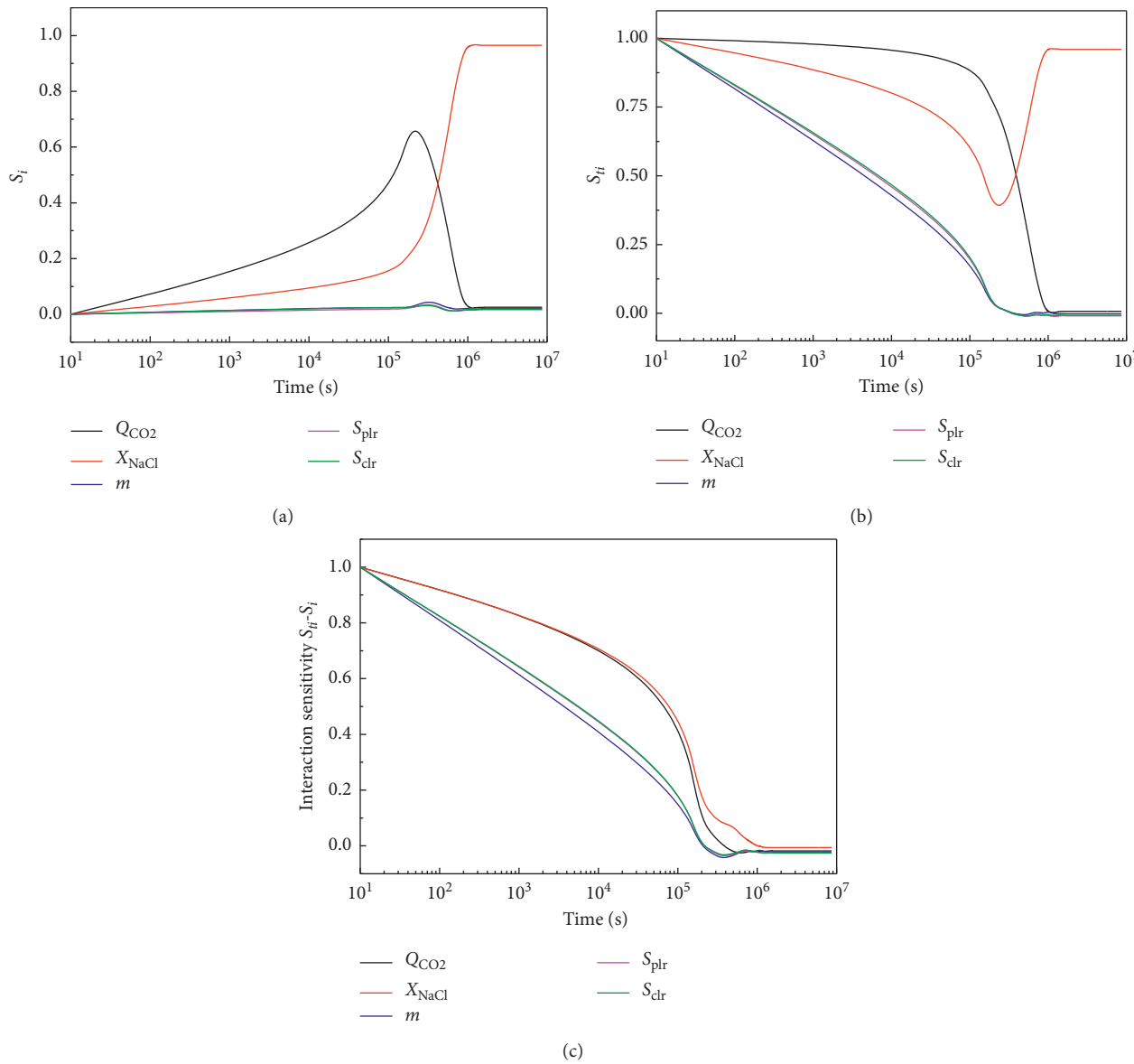

Figure 12: Time evolution of the sensitivity index: (a) S_i; (b) S_{ti}; (c) S_{ti}-S_i.

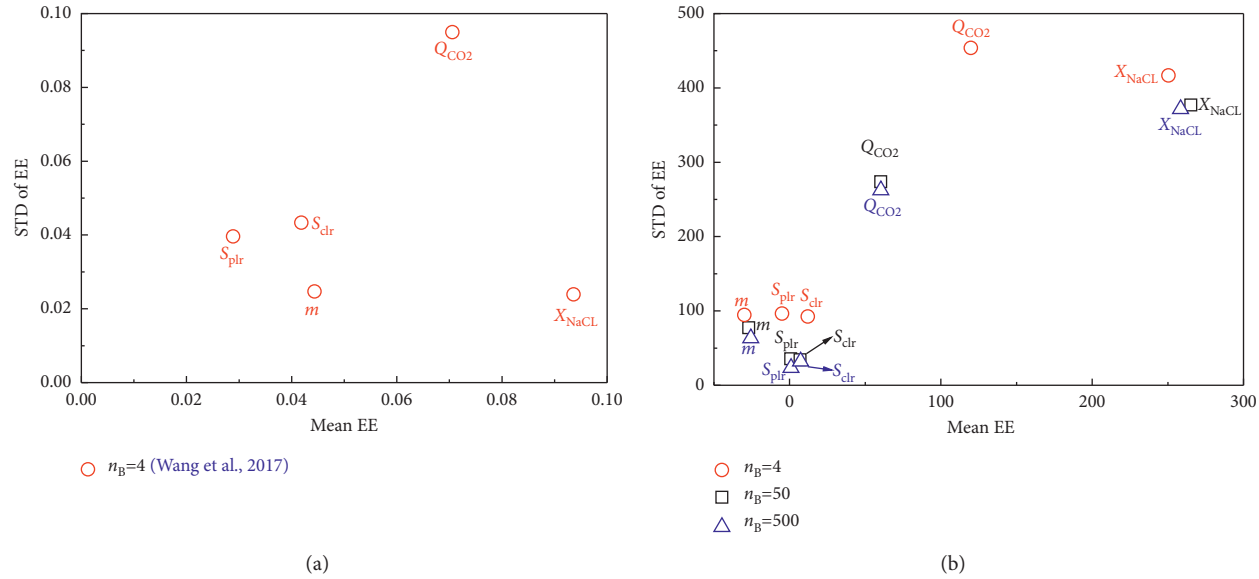

FIGURE 13: Morris global sensitivity analysis of S_s near the injection well: (a) STD of EE versus mean EE at 100 days with 4 paths [32]; (b) STD of EE versus mean EE at 100 days, the circles, squares, and triangles represent 4 paths, 50 paths, and 500 paths, respectively.

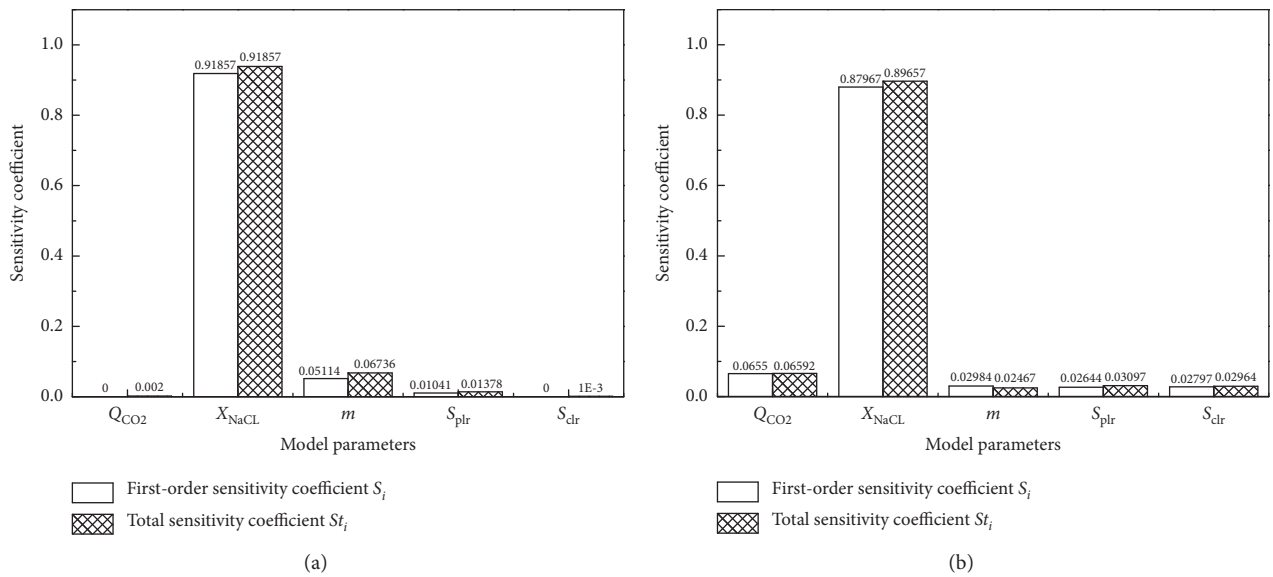

FIGURE 14: Continued.

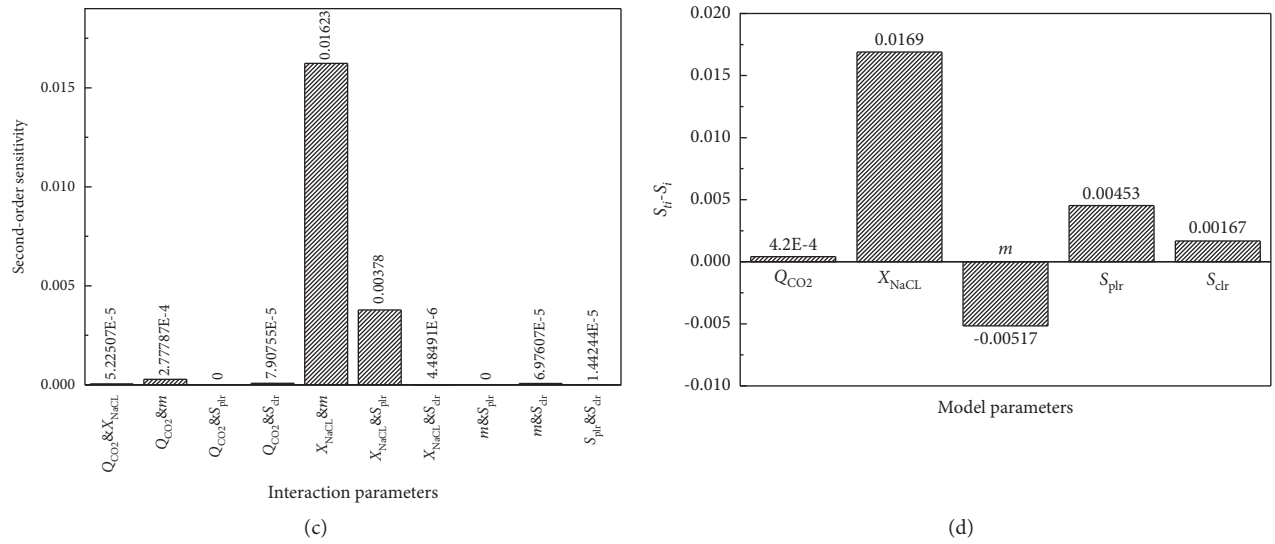

FIGURE 14: Sobol global sensitivity analysis of S_s near the injection well: (a) first-order and total sensitivity coefficients of the salting-out model in Wang et al. [32]; (b) set: 2,000, first-order, and total sensitivity index of the salting-out model with 14,000 simulations; (c) second-order sensitivity coefficient of the salting-out model in Wang et al. [32]; (d) interaction effect for all parameters.

about the sensitivity coefficient. X_{NaCl} has the greatest influence on the response variable S_s, much higher than the other parameters. The descending ranking of the sensitivity coefficient is X_{NaCl}, m, S_{plr}, Q_{CO2}, and S_{clr} in Figure 14(a); however, Figure 14(b) shows the different range of the sensitivity coefficient: X_{NaCl}, Q_{CO2}, S_{plr}, m, and S_{clr}. Q_{CO2} has the second place in this article but the lowest position in Wang et al. [32]. In this paper, the Morris method and the Sobol method get a similar sensitivity coefficient; what else the sensitivity coefficient result from Sobol method in this paper can also correspond to the sensitivity coefficient of the Morris method in Wang et al. The difference in results can be attributed to the use of the surrogate model and the number of simulations, full of simplicity and experience.

Figure 14(c) shows the contribution of the parameter interaction to the sensitivity, which is called the second-order sensitivity coefficient [32]. Interaction parameters that can be considered include X_{NaCl} and m, X_{NaCl} and S_{plr}, and Q_{CO2} and m. In Figure 14(d), the difference between S_{ti} and S_i identifies the interaction effect. X_{NaCl} has the biggest interaction effect, m and S_{plr} have a dominant interaction effect afterward, and Q_{CO2} has the smallest interaction effect. The results in Figure 14(c) and Figure 14(d) are consistent, but the difference between S_{ti} and S_i is much easier to get than the second-order sensitivity coefficient.

4. Conclusions

The sensitivity analysis of the salting-out effect on well injectivity is a significant work in the study of geological storage of CO_2 in deep saline aquifers, which is helpful in the selection of storage sites and the design of the injection strategy. In this study, we conduct a more detailed sensitivity analysis using the salting-out model, which includes the local sensitivity method and two global sensitivity methods. The main conclusions obtained from this study are as follows:

(1) Morris sensitivity coefficient requires several hundred and Sobol's sensitivity coefficient requires several thousand sampling matrices to stabilize in this study. The stability and accuracy of sensitivity calculation are related to the selection of calculation times, which cannot be selected according to experience but should be chosen to make the sensitivity coefficient converge.

(2) The sensitivity coefficient would change with the evaluation time. X_{NaCl} has always been the most important factor affecting salting out, and the parameters m, S_{plr}, and S_{clr} have low sensitivity. However, the less sensitive parameter Q_{CO2} at the end of the evaluation time has a dominant effect during the evaluation process. This indicated that the law of time evolution cannot be ignored when studying the physical process of the problem, which is a long-time accumulation process, such as the salting-out process in this study.

(3) Local sensitivity is a simplification of Morris, which can quickly select the most sensitive parameters. The Morris method is suitable for qualitatively selecting the most sensitive parameters and can obtain the interaction effect or the nonlinear effect. Sobol can quantify the sensitivity coefficient and cross-sensitivity coefficient, and it can help to compare with the Morris method to understand the nonlinear effect. The ranking of low sensitivity parameters (m, S_{plr}, and S_{clr}) importance is not easily recognized using Sobol's method; more simulations are required to rank low sensitivity parameters.

(4) Using the surrogate model to calculate the Sobol coefficient may cause some errors and uncertainty. Possible errors and uncertainties should be evaluated before the surrogate model is adopted to simplify the computation. On the other hand, the interaction

sensitivity expressed by the S_{ti}-S_i approximation without calculating the second-order coefficient is effective.

Nomenclature

d_i: Sensitivity coefficient in traditional sensitivity calculated method
k_x, k_y, k_z: Permeability in three directions
m: Parameter related to pore size distribution
n_B: The number of parameter paths
n_k: The number of parameters
n_p: The number of sampling points
n_s: The number of parameters sets
P: Pressure
P_0: Gas entry pressure
P_{max}: Maximum capillary pressure
Q_{CO2}: Injection rate of CO_2
S_{gas}: Gas saturation
S_{gr}: Residual gas saturation
S_i: First-order sensitivity coefficient in Sobol method
S_i^{local}: Local sensitivity coefficient
S_{lr}: Residual liquid saturation
S_{ls}: Liquid saturation in the saturated state
S_s: Solid saturation
S_{ti}: Total sensitivity coefficient in Sobol method
T: Temperature
x_i: Input parameter
X_{NaCl}: Salinity
ϕ: Porosity.

Data Availability

All the data generated or analyzed during this study are included in this published article.

Conflicts of Interest

The authors declare that there are no conflicts of interest regarding the publication of this paper.

Acknowledgments

The research was supported by the Jiangsu Planned Projects for Postdoctoral Research Funds (no. 2020Z006).

References

[1] S. Pye, F. G. N. Li, J. Price, and B. Fais, "Achieving net-zero emissions through the reframing of UK national targets in the post-Paris Agreement era," *Nature Energy*, vol. 2, Article ID 17024, 2017.

[2] D. Zhu, S. Peng, S. Zhao, M. Wei, and B. Bai, "Comprehensive review of sealant materials for leakage remediation technology in geological CO2 capture and storage process," *Energy and Fuels*, vol. 35, no. 6, pp. 4711–4742, 2021.

[3] Asian Development Bank, *Roadmap for Carbon Capture and Storage Demonstration and Deployment in the People's Republic of China*, Asian Development Bank, Mandaluyong City, PH, USA, 2015, https://www.adb.org/publications/roadmap-carbon-capture-and-storage-demonstration-and-deployment-prc.

[4] E. Ajoma, S. Saira, S. Thanarat, and L. Furqan, "Effect of miscibility and injection rate on water-saturated CO2 Injection," *Energy*, vol. 217, 2021.

[5] G. Cui, L. Yang, J. Fang, Z. Qiu, Y. Wang, and S. Ren, "Geochemical reactions and their influence on petrophysical properties of ultra-low permeability oil reservoirs during water and CO2 flooding," *Journal of Petroleum Science and Engineering*, vol. 203, Article ID 108672, 2021.

[6] N. Spycher, K. Pruess, and J. Ennis-King, "CO2-H2O mixtures in the geological sequestration of CO2. I. assessment and calculation of mutual solubilities from 12 to 100°C and up to 600 bar," *Geochimica et Cosmochimica Acta*, vol. 67, no. 16, pp. 3015–3031, 2003.

[7] Y. Cinar and A. Riaz, "Carbon dioxide sequestration in saline formations: part 2-review of multiphase flow modeling," *Journal of Petroleum Science and Engineering*, vol. 124, pp. 381–398, 2014.

[8] M. Gao, J. Xie, J. Guo, Y. Lu, Z. He, and C. Li, "Fractal evolution and connectivity characteristics of mining-induced crack networks in coal masses at different depths," *Geomechanics and Geophysics for Geo-Energy and Geo-Resources*, vol. 7, no. 1, pp. 1–15, 2021.

[9] M. Gao, J. Xie, Y. Gao et al., "Mechanical behavior of coal under different mining rates: a case study from laboratory experiments to field testing," *International Journal of Mining Science and Technology*, vol. 31, no. 5, pp. 825–841, 2021.

[10] J. M. Nordbotten, M. A. Celia, and S. Bachu, "Injection and storage of CO2 in deep saline aquifers: analytical solution for CO2 plume evolution during injection," *Transport in Porous Media*, vol. 58, no. 3, pp. 339–360, 2005.

[11] Y. D. Oruganti and S. Mishra, "An improved simplified analytical model for CO2 plume movement and pressure buildup in deep saline formations," *International Journal of Greenhouse Gas Control*, vol. 14, pp. 49–59, 2013.

[12] X. Yu, M. Ahmadinia, S. M. Shariatipour, D. Lawton, K. Osadetz, and A. Saeedfar, "Impact of reservoir permeability, permeability anisotropy and designed injection rate on CO2 gas behavior in the shallow saline aquifer at the CaMI field research station, brooks, alberta," *Natural Resources Research*, vol. 29, no. 4, pp. 2735–2752, 2020.

[13] Y. Diao, G. Zhu, X. Li et al., "Characterizing CO2 plume migration in multi-layer reservoirs with strong heterogeneity and low permeability using time-lapse 2D VSP technology and numerical simulation," *International Journal of Greenhouse Gas Control*, vol. 92, Article ID 102880, 2020.

[14] H. Erfani, M. Babaei, and V. Niasar, "Dynamics of CO2 density-driven flow in carbonate aquifers: effects of dispersion and geochemistry," *Water Resources Research*, vol. 57, no. 4, Article ID e2020WR027829, 2021.

[15] G. Baumann, J. Henninges, and M. De Lucia, "Monitoring of saturation changes and salt precipitation during CO 2 injection using pulsed neutron-gamma logging at the Ketzin pilot site," *International Journal of Greenhouse Gas Control*, vol. 28, pp. 134–146, 2014.

[16] A. Verma and K. Pruess, "Thermohydrological conditions and silica redistribution near high-level nuclear wastes emplaced in saturated geological formations," *Journal of Geophysical Research*, vol. 93, no. B2, pp. 1159–1173, 1988.

[17] K. Pruess, *ECO2N: A TOUGH2 Fluid Property Module for Mixtures of Water, NaCl, and CO2*, Lawrence Berkeley Laboratory Report, Berkeley, CA, USA, 2005.

[18] R. Miri and H. Hellevang, "Salt precipitation during CO 2 storage-a review," *International Journal of Greenhouse Gas Control*, vol. 51, pp. 136–147, 2016.

[19] T. Giorgis, M. Carpita, and A. Battistelli, "2D modeling of salt precipitation during the injection of dry CO2 in a depleted gas reservoir," *Energy Conversion and Management*, vol. 48, no. 6, pp. 1816–1826, 2007.

[20] M. Zeidouni, M. Pooladi-Darvish, and D. Keith, "Sensitivity analysis of salt precipitation and CO2-brine displacement in Saline Aquifers, society of petroleum engineers," in *Proceedings of the SPE International Conference On CO2 Capture, Storage, and Utilization*, San Diego, CA, USA, November 2009.

[21] K.-Y. Kim, W. S. Han, J. Oh, T. Kim, and J.-C. Kim, "Characteristics of salt-precipitation and the associated pressure build-up during CO2 storage in saline aquifers," *Transport in Porous Media*, vol. 92, no. 2, pp. 397–418, 2012.

[22] Y. Wang and Y. Liu, "Impact of capillary pressure on permeability impairment during CO2 injection into deep saline aquifers," *Journal of Central South University*, vol. 20, no. 8, pp. 2293–2298, 2013.

[23] L. André, Y. Peysson, and M. Azaroual, "Well injectivity during CO2 storage operations in deep saline aquifers - Part 2: numerical simulations of drying, salt deposit mechanisms and role of capillary forces," *International Journal of Greenhouse Gas Control*, vol. 22, pp. 301–312, 2014.

[24] K. Pruess and N. Müller, "Formation dry-out from CO2 injection into saline aquifers: 1. Effects of solids precipitation and their mitigation," *Water Resources Research*, vol. 45, no. 3, Article ID W03402, 2009.

[25] Y. Wang and Y. Liu, "Dry-out effect and site selection for CO2 storage in deep saline aquifers," *Rock and Soil Mechanics*, vol. 35, no. 6, pp. 1711–1717, 2014.

[26] M. D. Morris, "Factorial sampling plans for preliminary computational experiments," *Technometrics*, vol. 33, no. 2, pp. 161–174, 1991.

[27] I. M. Sobol', "Global sensitivity indices for nonlinear mathematical models and their Monte Carlo estimates," *Mathematics and Computers in Simulation*, vol. 55, no. 1, pp. 271–280, 2001.

[28] Y. Jung, Q. Zhou, and J. T. Birkholzer, "Early detection of brine and CO2 leakage through abandoned wells using pressure and surface-deformation monitoring data: concept and demonstration," *Advances in Water Resources*, vol. 62, pp. 555–569, 2013.

[29] H. M. Wainwright, S. Finsterle, Y. Jung, Q. Zhou, and J. T. Birkholzer, "Making sense of global sensitivity analyses," *Computers & Geosciences*, vol. 65, pp. 84–94, 2014.

[30] F. Zheng, X. Shi, J. Wu, L. Zhao, and C. Wang, "Global sensitivity analysis of leakage risk for CO2 geological sequestration in the saline aquifer of yancheng formation in subei basin," *Geological Journal of China Universities*, vol. 18, no. 2, pp. 232–238, 2012.

[31] F. Zheng, X. Shi, J. Wu, L. Zhao, and Y. Cheng, "Global parametric sensitivity analysis of numerical simulation for CO2 geological sequestration in saline aquifers: a case study of yancheng formation in subei basin," *Journal of Jilin University (Earth Science Edition)*, vol. 44, no. 1, pp. 310–318, 2014.

[32] Y. Wang, J. Ren, S. Hu, and D. Feng, "Global sensitivity analysis to assess salt precipitation for CO2," *Geological Storage in Deep Saline Aquifers*, Geofluids, vol. 2017, Article ID 5603923, 16 pages, 2017.

[33] G. Cui, W. Wang, B. Dou et al., "Geothermal energy exploitation and power generation via a single vertical well combined with hydraulic fracturing," *Journal of Energy Engineering*, vol. 148, no. 1, Article ID 04021058, 2022.

[34] X. Li, K. Peng, J. Peng, and H. Xu, "Effect of cyclic wetting-drying treatment on strength and failure behavior of two quartz-rich sandstones under direct shear," *Rock Mechanics and Rock Engineering*, vol. 54, no. 11, pp. 5953–5960, 2021.

[35] C. Zhu, M. He, M. Karakus, X. Zhang, and Z. Tao, "Numerical simulations of the failure process of anaclinal slope physical model and control mechanism of negative Poisson's ratio cable," *Bulletin of Engineering Geology and the Environment*, vol. 80, no. 4, pp. 3365–3380, 2021.

[36] Z. Tao, Q. Geng, C. Zhu et al., "The mechanical mechanisms of large-scale toppling failure for counter-inclined rock slopes," *Journal of Geophysics and Engineering*, vol. 16, no. 3, pp. 541–558, 2019.

[37] Y. Mualem, "A new model for predicting the hydraulic conductivity of unsaturated porous media," *Water Resources Research*, vol. 12, no. 3, pp. 513–522, 1976.

[38] M. T. van Genuchten, "A closed-form equation for predicting the hydraulic conductivity of unsaturated soils," *Soil Science Society of America Journal*, vol. 44, no. 5, pp. 892–898, 1980.

[39] G. Bacci, A. Korre, and S. Durucan, "Experimental investigation into salt precipitation during CO2 injection in saline aquifers," *Energy Procedia*, vol. 4, pp. 4450–4456, 2011.

[40] Y. Peysson, L. André, and M. Azaroual, "Well injectivity during CO2 storage operations in deep saline aquifers-Part 1: experimental investigation of drying effects, salt precipitation and capillary forces," *International Journal of Greenhouse Gas Control*, vol. 22, pp. 291–300, 2014.

[41] K. Pruess, C. Oldenburg, and G. Moridis, *Tough2 User's Guide, Version 2*, Lawrence Berkeley Laboratory Report, Berkeley, CA, USA, 2012.

[42] M. C. Hill and C. R. Tiedeman, *Effective Groundwater Model Calibration: With Analysis of Data, Sensitivities, Predictions, and Uncertainty*, John Wiley & Sons, J, USA, 2007.

[43] A. Saltelli, M. Ratto, T. Andres et al., "Sensitivity analysis: from theory to practice," in *Global Sensitivity Analysis. The Primer*John Wiley & Sons, Hoboken, NJ, 2007.

[44] A. Saltelli, S. Tarantola, F. Campolongo, and M. Ratto, *Sensitivity Analysis in Practice: A Guide to Assessing Scientific Models*, John Wiley & Sons, Hoboken, NJ, 2004.

[45] H. M. Wainwright, S. Finsterle, Q. Zhou, and J. T. Birkholzer, "Modeling the performance of large-scale CO2 storage systems: a comparison of different sensitivity analysis methods," *International Journal of Greenhouse Gas Control*, vol. 17, pp. 189–205, 2013.

[46] S. Finsterle, "Practical notes on local data-worth analysis," *Water Resources Research*, vol. 51, no. 12, pp. 9904–9924, 2015.

[47] M. C. Hill and C. R. Tiedeman, *Effective Groundwater Model Calibration: With Analysis of Data, Sensitivities, Predictions, and Uncertainty*, John Wiley & Sons, Hoboken, NJ, USA, 2006.

[48] S. N. Lophaven, H. B. Nielsen, and J. Søndergaard, *DACE: A Matlab Kriging Toolbox. IMM, Informatics And Mathematical Modelling*, The Technical University of Denmark, Lyngby, Denmark, 2002.

[49] C.-C. Chang and C.-J. Lin, "Libsvm," *ACM transactions on intelligent systems and technology*, vol. 2, no. 3, pp. 1–27, 2011.